American Journal of Mathematics and Physics Application
ISSN: 2290-8887
Volume 01, Issue 03, October, 2019

Turbulence Birth from Poiseuille Flow Curvature

Franck Delplace[1]
ESI Group Scientific Committee, 100 Av. De Suffren, Paris, France[1]

Abstract— In this paper, we considered the well-known parabolic velocity field of Poiseuille flow, as a Riemannian manifold. Calculations of both first and second fundamental forms allowed mean and Gauss curvatures of the paraboloid of revolution, to be calculated. From the Lamb form of Navier-Stokes equation, we calculated both the flexion product and enstrophy giving the Lamb vector divergence as a function of Gauss curvature of the laminar velocity field. These results allowed the stability of Poiseuille flow to be investigated through the influence of maximum flow curvature and the Lamb vector divergence. We showed that classical critical Reynolds number approach is not enough to explain the change from laminar to transition flow regime. A new method, based on Gauss curvature calculation of the Riemannian manifold is then proposed.

Keywords— Turbulence – Poiseuille – Curvature – Gauss – Reynolds – Navier-Stokes - Lamb

1. Introduction

In fluid dynamics, the Hagen-Poiseuille equation gives the pressure drop, in an incompressible Newtonian liquid, flowing in the laminar flow regime, in a long cylindrical pipe of constant cross-section. This important experimental result, obtained independently by Jean Léonard Marie Poiseuille in 1838 and Gotthilf Heinrich Ludwig Hagen, showed that pressure drop $\Delta p(Pa)$ is proportional to liquid flow-rate $Q(m^3.s^{-1})$. The proportionality constant is a function of geometrical parameters (pipe length $L(m)$ and radius $R(m)$) and the liquid dynamic viscosity $\eta(Pa.s)$ [1]:

$$\Delta p = \frac{8\,L\,\eta}{\pi\,R^4}\,Q \quad (1)$$

Solving Navier-Stokes (NS) equation, in the fully established laminar flow regime, in the case of a cylindrical duct of circular cross-section, is quite easy and it gives a parabolic velocity field, or more accurately a paraboloid of revolution (POR) as represented in the following figure.

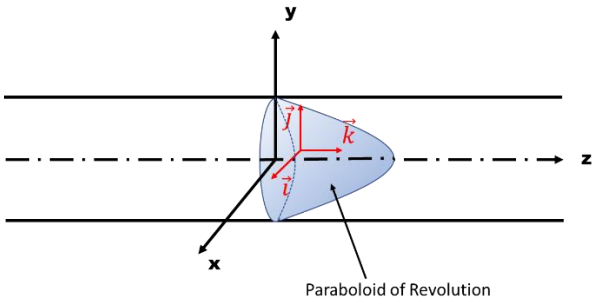

FIGURE 1: Laminar flow velocity field giving a paraboloid of revolution.

For ducts of non-circular cross-section, this problem becomes rapidly much more complex, and as an example, solutions of NS equation for rectangular ducts involves series of hyperbolic functions [2].

For the mathematicians, the POR can be considered as a smooth Riemannian manifold (M, g) with its metric tensor $\boldsymbol{g_{ij}}$ (the first fundamental form) which allows Euclidian distance to be generalized to curved spaces. As reported by Villani [3], curvature is the basis of non-Euclidian geometry. First introduced by Gauss and

further developed by Riemann, curvature measures the degree of non-Euclidian behaviour in geodesics.

According to [3], the main purpose of this paper is to study the laminar flow velocity field shape in a pipe, using curvature of Riemannian manifolds definitions. We will begin by giving detailed calculations of first and second fundamental forms, for the well-known case of a circular cross-section giving the POR illustrated in figure 1. From these results, giving principal curvatures as the eigenvalues of second fundamental form, we will try to make the link with NS equation and particularly with the famous unsolved problem of laminar shear flow stability.

As reported in [4-8], the change from laminar to transition and turbulent flow regime is characterized by critical Reynolds number (Re_c) values. In a pipe of circular cross-section, Re_c is experimentally found to vary in a wide range i.e. from 2000 to 100 000 [8]. Moreover, as reported by Delplace [4], Re_c values in regular ducts depend on cross-section geometry making this problem extremely complicated. As written by Durst et al. [9], "there is no clear picture of what causes the flow to go from the laminar to the turbulent state in pipe flows". In their experiments, carried out with air flowing in a brass pipe of 15 mm diameter, these authors were able to maintain a laminar flow up to $Re = 13000$ which is a quite high value compared to the usual value $Re = 2300$ often obtained with water.

In a second chapter, we will use the Lamb form of NS equation [7] to build a relationship between the Lamb vector divergence and the topology of the POR described by its Gauss curvature. Of course, the shape of the POR changes as the Reynolds number increases and the Gauss curvature naturally appears a good way to measure these changes. From the study of Gauss curvature function, we will investigate the evolution of both the Lamb vector divergence and local Gauss curvature, as Reynolds number increases to reach the transition flow region.

Finally, from these results analysis, we will propose an original explanation of fluids flow stability in pipes which could be extended to all flows in closed or open channels.

2. Curvature of Poiseuille flow velocity field.

From NS equation, and using Cartesian coordinates with basis vectors $\boldsymbol{i}, \boldsymbol{j}, \boldsymbol{k}$ (figure 1), we have:

$$\eta\left(\frac{\partial^2 u_z}{\partial x^2}+\frac{\partial^2 u_z}{\partial y^2}\right)\boldsymbol{k}=\frac{\partial p_z}{\partial z}\boldsymbol{k} \quad (2)$$

With η $(Pa.s)$ the liquid dynamic viscosity, u_z $(m.s^{-1})$ the velocity in the flow direction z and p_z (Pa) the pressure in the pipe. Considering symmetry, we can write:

$$\frac{\partial^2 u_z}{\partial r^2}=-\frac{\Delta p}{2\eta L} \quad (3)$$

Where r and L are respectively radius and pipe length and Δp (Pa) the pressure drops. Integration of equation (3), with boundary conditions $u_z(R)=0$ and $(\partial u_z/\partial r)_{r=0}=0$, gives well-known parabolic velocity field:

$$u_z(r)=\frac{\Delta p}{4\eta L}(R^2-r^2)=u_{max}\left(1-\frac{r^2}{R^2}\right)=2\overline{u}\left(1-\frac{r^2}{R^2}\right) \quad (4)$$

$R(m)$ is the circular cross-section radius, u_{max} is the maximum velocity at duct centre, and $\overline{u}$ is the liquid mean velocity.

Let us now consider the POR (M, g) as a surface immersed in $\mathbb{R}^3$ with Cartesian coordinates as represented in the following figure.

American Journal of Mathematics and Physics Application
ISSN: 2290-8887
Volume 01, Issue 03, October, 2019

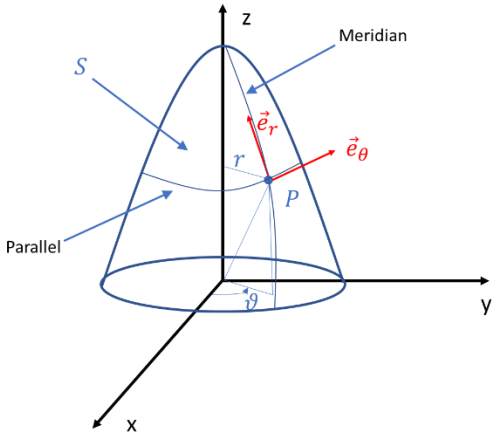

FIGURE 2: The paraboloid of revolution immersed in $\mathbb{R}^3$.

Parametric equations of surface *S* are given by:

$$\begin{cases} x = rcos\theta \\ y = rsin\theta \\ z = r^2/2m \end{cases} \quad (5)$$

With $z = u_{max} - u_z(r)$ and $1/2m = u_{max}/R^2$ coming from equation (4). To avoid dimensions problems, we should write: $z = h_{max} - h(r)$ and $1/2m = h_{max}/R^2$ where h represents the high of the velocity vector or its norm. At the centre of the duct, we have: $r = 0$ giving $u_z(r) = u_z(0) = u_{max}$ or $h(r) = h(0) = h_{max}$. $\forall\ P\ \in S$ (Figure 2), we can define the local orthogonal basis associated to *P* as followed:

$$\boldsymbol{e_r} = \frac{\partial \boldsymbol{r}}{\partial r} = \begin{pmatrix} cos\theta \\ sin\theta \\ r/m \end{pmatrix} and\ \boldsymbol{e_\theta} = \frac{\partial \boldsymbol{r}}{\partial \theta} = \begin{pmatrix} -rsin\theta \\ rcos\theta \\ 0 \end{pmatrix} \quad (6)$$

$\boldsymbol{e_r}$ vectors are tangent to the meridians which are parabolas given by equation (4) and $\boldsymbol{e_\theta}$ vectors are tangent to the parallels which are circles of radius r (see figure 2).

From this parametrization of Riemannian manifold (M, g), we can calculate the metric tensor g_{ij} often called the first fundamental form.

$(\boldsymbol{e_r};\ \boldsymbol{e_\theta})$ being an orthogonal basis, we have $g_{12} = g_{21} = 0$.
$g_{11} = \boldsymbol{e_r}\,.\,\boldsymbol{e_r} = 1 + r^2/m^2$
$g_{22} = \boldsymbol{e_\theta}\,.\,\boldsymbol{e_\theta} = r^2$
Giving,

$$\boldsymbol{g_{ij}} = \begin{pmatrix} g_{11} & g_{12} \\ g_{21} & g_{22} \end{pmatrix} = \begin{pmatrix} 1 + \frac{r^2}{m^2} & 0 \\ 0 & r^2 \end{pmatrix} \quad (7)$$

And,

$det(\boldsymbol{g_{ij}}) = g = \frac{r^2}{m^2}(m^2 + r^2)$ (8)

$\sqrt{g} = |\boldsymbol{e_r} \times \boldsymbol{e_\theta}| = \frac{r}{m}\sqrt{m^2 + r^2}$ (9)

Let us now establish the second fundamental form we called b_{ij}:
Using well-known definition:

$$\boldsymbol{b_{ij}} = \boldsymbol{e_{i,j}} \,.\, \boldsymbol{n} \quad (10)$$

Where $\boldsymbol{n}$ is a unit vector normal to the Riemannian manifold surface. We must then calculate the derivatives of basis vectors $(\boldsymbol{e_r};\ \boldsymbol{e_\theta})$:

$$\frac{\partial \boldsymbol{e_r}}{\partial r} = \begin{pmatrix} 0 \\ 0 \\ 1/m \end{pmatrix};\ \frac{\partial \boldsymbol{e_r}}{\partial \theta} = \begin{pmatrix} -sin\theta \\ cos\theta \\ 0 \end{pmatrix};\ \frac{\partial \boldsymbol{e_\theta}}{\partial r} = \begin{pmatrix} -sin\vartheta \\ cos\vartheta \\ 0 \end{pmatrix};\ \frac{\partial \boldsymbol{e_\theta}}{\partial \vartheta} = \begin{pmatrix} -rcos\vartheta \\ -rsin\vartheta \\ 0 \end{pmatrix} \quad (11)$$

The normal unit vector $\boldsymbol{n}$ is defined by:

$$\boldsymbol{n} = \frac{\boldsymbol{e_r} \times \boldsymbol{e_\theta}}{|\boldsymbol{e_r} \times \boldsymbol{e_\theta}|} = \frac{\boldsymbol{e_r} \times \boldsymbol{e_\theta}}{\sqrt{g}} \quad (12)$$

And,

$$\boldsymbol{e_r} \times \boldsymbol{e_\theta} = \begin{pmatrix} -\frac{r^2}{m} cos\theta \\ -\frac{r^2}{m} sin\theta \\ r \end{pmatrix} \quad (13)$$

Using equations (9) and (12), we obtain:

$$\boldsymbol{n} = \frac{m}{r\sqrt{(m^2 + r^2)}} \begin{pmatrix} -\frac{r^2}{m} cos\theta \\ -\frac{r^2}{m} sin\theta \\ r \end{pmatrix} \quad (14)$$

Finally, from equation (10), we obtain the second fundamental form, being a second order covariant tensor:

$$\boldsymbol{b_{ij}} = \frac{m}{r\sqrt{(m^2 + r^2)}} \begin{pmatrix} \frac{r}{m} & 0 \\ 0 & \frac{r^3}{m} \end{pmatrix} \quad (15)$$

From equations (7) and (15), we see that both first and second fundamental forms are diagonal; the coordinate lines (meridians and parallels) are orthogonal, and they form lines of curvature i.e., they locally coincide with the principal directions of curvature. The directions along which, the normal curvature is extremal, are given by the eigenvectors of matrix $\boldsymbol{b_i^j}$, and the corresponding eigenvalues are the extremal curvatures. We have then to calculate $\boldsymbol{b_i^j}$ using tensorial calculus rules:

$\boldsymbol{b_i^j} = \boldsymbol{b_{ik}} \boldsymbol{g^{kj}}$ (16)

And,

$$\boldsymbol{g^{ij}} = \begin{pmatrix} g^{11} & g^{12} \\ g^{21} & g^{22} \end{pmatrix} = \frac{1}{g} \begin{pmatrix} g_{22} & 0 \\ 0 & g_{11} \end{pmatrix} = \frac{m^2}{r^2(m^2 + r^2)} \begin{pmatrix} r^2 & 0 \\ 0 & 1 + \frac{r^2}{m^2} \end{pmatrix} \quad (17)$$

From equations (15), (16) and (17), we obtain:

$$\boldsymbol{b_i^j} = \frac{m^3\sqrt{m^2 + r^2}}{r^3(m^2 + r^2)^2} \begin{pmatrix} \frac{r^3}{m} & 0 \\ 0 & \frac{r^3(m^2 + r^2)}{m^3} \end{pmatrix} = \begin{pmatrix} \frac{m^2\sqrt{m^2 + r^2}}{(m^2 + r^2)^2} & 0 \\ 0 & \frac{\sqrt{m^2 + r^2}}{(m^2 + r^2)} \end{pmatrix} \quad (18)$$

This important result gives the two eigenvalues, which are the principal curvatures of the POR. We called κ_1 and κ_2 these principal curvatures:

$$\kappa_1 = b_1^1 = \frac{m^2\sqrt{m^2+r^2}}{(m^2+r^2)^2} \quad (19)$$

$$\kappa_2 = b_2^2 = \frac{\sqrt{m^2+r^2}}{(m^2+r^2)} \quad (20)$$

At the centre of the duct, i.e. for $r = 0$ we have $\kappa_1 = \kappa_2 = 1/m$. This point is often called an umbilic.
Mean curvature H, and Gauss curvature K, are defined respectively as sum and product of principal curvatures giving:

$$2H = \kappa_1 + \kappa_2 = \frac{\sqrt{m^2+r^2}\,(2m^2+r^2)}{(m^2+r^2)^2} \quad (21)$$

$$K = \kappa_1 . \kappa_2 = \frac{m^2}{(m^2+r^2)^2} \quad (22)$$

It is then possible, from above equations, to calculate $2H$ and K at $r = 0$ i.e. at the centre of the duct which corresponds to maximum POR curvature and also to the umbilic.

$$(2H)_{r=0} = \frac{2}{m} \quad (23)$$

$$(K)_{r=0} = \frac{1}{m^2} \quad (24)$$

And, using parametrization of the POR given at the beginning of this chapter, i.e. $\frac{1}{2m} = h_{max}/R^2$, we obtain:

$$(2H)_{r=0} = \frac{4h_{max}}{R^2} \quad (25)$$

$$(K)_{r=0} = \frac{4h_{max}^2}{R^4} \quad (26)$$

With of course h_{max} corresponding to $u_{max} = 2\bar{u}$ in our velocity field parametrization given at the beginning of this chapter.

3. Analysis using Lamb form of NS equation.

3.1 Theory.

As clearly reported in [7], the Lamb form of NS equation for an incompressible fluid is derived from classical NS equation formulation:

$$\frac{D\boldsymbol{u}}{Dt} = \frac{\partial \boldsymbol{u}}{\partial t} + \boldsymbol{u}.\boldsymbol{\nabla u} = -\frac{1}{\rho}\boldsymbol{\nabla} \mathrm{p} + \nu\Delta(\boldsymbol{u}) \; with \; \boldsymbol{\nabla}.\boldsymbol{u} = 0 \quad (27)$$

Where ρ is the fluid density and ν the kinematic viscosity.

Using Lamb vector definition i.e. $\boldsymbol{l} = \boldsymbol{\omega} \times \boldsymbol{u}$, with $\boldsymbol{\omega}$ the vorticity vector defined as the curl of the velocity vector: $\boldsymbol{\omega} = \boldsymbol{\nabla} \times \boldsymbol{u}$, we obtain the Lamb form of NS equation:

$$\frac{\partial \boldsymbol{u}}{\partial t} + \boldsymbol{l} = -\boldsymbol{\nabla}\Phi - \nu(\boldsymbol{\nabla} \times \boldsymbol{\omega}) \quad (28)$$

With Φ, the scalar quantity often called the Bernoulli function [7] and defined as followed:

$$\Phi = \frac{p}{\rho} + \frac{\boldsymbol{u}^2}{2} \quad (29)$$

Taking the divergence of equation (28) gives, for an incompressible fluid ($\boldsymbol{\nabla}.\boldsymbol{u} = 0$), the following relationship between the Lamb vector divergence and the Bernoulli function [7]:

$$\boldsymbol{\nabla}.\boldsymbol{l} = -\Delta\Phi \quad (30)$$

This equation is a Poisson partial differential equation which gives an important relationship between the curvature of the flow energy field (through the scalar Laplacian) and the divergence of the Lamb vector.

As reported in [7], the divergence of the Lamb vector is then a scalar quantity of major importance also defined by:

$$\boldsymbol{\nabla}.\boldsymbol{l} = \boldsymbol{u}.(\boldsymbol{\nabla}\times\boldsymbol{\omega}) - \boldsymbol{\omega}.\boldsymbol{\omega} \qquad (31)$$

Where the first term in the right side is the flexion product and the second term is the enstrophy.

3.2 Application to Poiseuille flow.

Poiseuille flow is a typical case of unidirectional shear flow with a parabolic velocity field described by equation (4). We can then use equation (31) to calculate the Lamb vector divergence as followed:

$$\boldsymbol{\nabla}.\boldsymbol{l} = -u_z\frac{\partial^2 u_z}{\partial r^2} - \left(\frac{\partial u_z}{\partial r}\right)^2 \qquad (32)$$

Calculations of first and second derivatives gives the following relationships for both the flexion product and enstrophy:

$$-u_z\frac{\partial^2 u_z}{\partial r^2} = \frac{2u_{max}^2}{R^4}(R^2 - r^2) \qquad (33)$$

$$\left(\frac{\partial u_z}{\partial r}\right)^2 = \frac{4u_{max}^2}{R^4}r^2 \qquad (34)$$

From analysis of the POR topology performed in chapter 2, we know that Gauss curvature at the centre of the pipe i.e. $(K)_{r=0}$ is given by equation (26). Let us now call this quantity K_{max} because it corresponds to the maximum curvature of the POR. We can then write the Lamb vector divergence as a function of K_{max}, giving:

$$\boldsymbol{\nabla}.\boldsymbol{l} = \frac{K_{max}}{2}(R^2 - r^2) - K_{max}r^2 \qquad (35)$$

We can then plot the evolution of flexion product, enstrophy and Lamb vector divergence vs the dimensionless ratio (r/R). We fixed $K_{max}R^2 = 100$ to obtain the following graph.

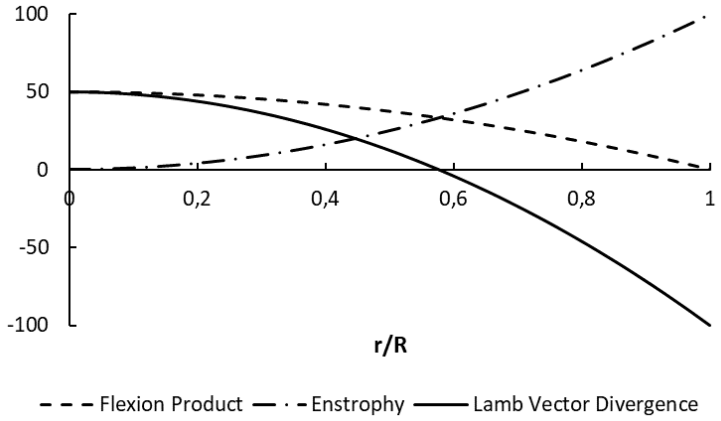

FIGURE 3: Flexion product, Enstrophy and $\boldsymbol{\nabla}.\boldsymbol{l}$ vs (r/R).

As reported in [7], evolution of $\boldsymbol{\nabla}.\boldsymbol{l}$ shows two regions. The first one, from the pipe centre to the point where $\boldsymbol{\nabla}.\boldsymbol{l} = 0$ and the second one from this point to the pipe wall. In the first region, $\boldsymbol{\nabla}.\boldsymbol{l} > 0$ and in the second one $\boldsymbol{\nabla}.\boldsymbol{l} < 0$. The transition between these two regions occurs at $r = R/\sqrt{3} \cong 0.577R$ and this value does not depend on K_{max} and then does not depend on the flow rate. As said in [7], the interaction between negative and positive regions of Lamb vector divergence as shown in figure 3 is a key characteristic of many complex flows.

American Journal of Mathematics and Physics Application
ISSN: 2290-8887
Volume 01, Issue 03, October, 2019

It is also worthwhile to notice the link between geometrical quantity $K_{max}R^2$ and extremal values of flexion product, enstrophy and Lamb vector divergence. Flexion product and Lamb vector divergence reach their maximum value $K_{max}R^2/2$ at the centre of the pipe and enstrophy reaches its maximum value $K_{max}R^2$ at the wall. Moreover, considering the POR as cylinders interlocking each other, calculation of the radius of the cylinder which offers the maximum viscous friction surface exactly corresponds to $r = R/\sqrt{3}$. This value corresponds to the crossing of flexion product and enstrophy curves and then to the null value of Lamb vector divergence. These results clearly show the deep link between the laminar Riemannian manifold topology and the Lamb vector divergence.

But the fact that the Lamb vector divergence null value position does not depend on the flow rate and then on the Reynolds number value makes this quantity not suitable to explain and quantify when the flow regime will change from laminar to transition. From friction curves experimentally obtained we know that the sudden change of the flow regime occurs for Reynolds number varying in the range 2000 to 100 000, depending on the disturbances that may affect fluid flow stability. The following friction curve obtained using Churchill's [9] well-known model and using $f = \tau_w/\rho\bar{u}^2$ clearly illustrates this change in the flow regime occurring for critical Reynolds number value $Re_c = 2300$.

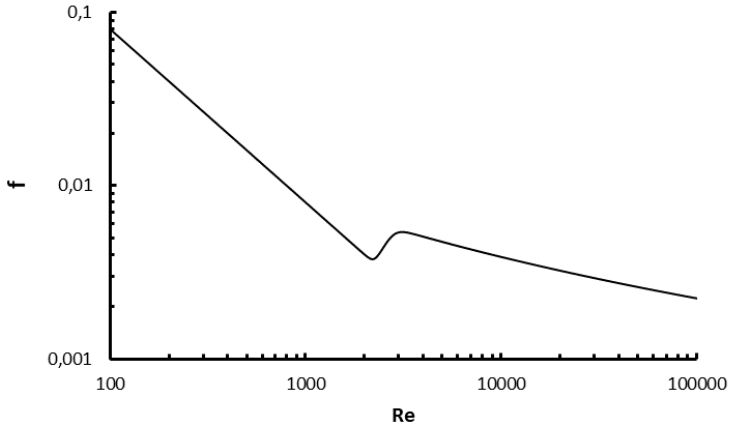

FIGURE 4: Friction curve given by Churchill's model [8].

From these considerations, even if the Lamb vector divergence or its opposite giving the energy field curvature through the Laplacian of Bernoulli function (equation 30) are important quantities for understanding of turbulent flow regime; it seems they cannot explain in deep why a shear flow or purely viscous flow will end giving rise to the first eddies and then to the transition flow regime. This flow instability starting at Re_c around 2000 and lasting up to 100 000 needs to be characterised by another parameter which is more intrinsic and equation (35) clearly indicates that Gauss curvature could be this quantity.

3.3 Gauss curvature as a function of pipe radius.

In chapter 2, we established the Gauss curvature of the POR in equation (22). It is then possible to calculate both first and second derivatives of function $K(r) = m^2/(m^2 + r^2)^2$:

$$\frac{dK(r)}{dr} = -\frac{4m^2 r}{(m^2 + r^2)^3} \qquad (36)$$

$$\frac{d^2K(r)}{dr^2} = m^2\left(\frac{24r^2}{(m^2 + r^2)^4} - \frac{4}{(m^2 + r^2)^3}\right) \qquad (37)$$

From the definition of parameter m in chapter 2, we have: $m^2 = 1/K_{max} = R^4/4u_{max}^2$ which allows function

$K(r)$ to be rewritten as follows:

$$K(r) = \frac{1/K_{max}R^4}{\left(\frac{1}{K_{max}R^2} + \left(\frac{r}{R}\right)^2\right)^2} \qquad (38)$$

From equation (36), function $K(r)$ reaches its maximum value K_{max} at the centre of the duct and then decreases as (r/R) increases. From equation (37), $K(r)$ can exhibit an inflexion point at $r = m/\sqrt{5} = 1/\sqrt{5K_{max}}$. This means that the shape of $K(r)$ function will change as the quantity $K_{max} = 4u_{max}^2/R^4$ and then the Reynolds number value will change. This important result could make Gauss curvature function a good candidate to explain fluids flow instability when Reynolds number value reaches the threshold of the transition flow regime. We will now examine in details the evolution of Gauss curvature function as Reynolds number increases.

4. Results and discussion.

4.1 Evolution of $K(r)$ with K_{max}.

We start this section by studying the change of $K(r)$ function shape as K_{max} increases from 10^3 to $10^6$and then the Reynolds number increases. To do that, we needed to fix a value of pipe radius R in equation (38). Most of the time, pipes radii are in the order of some centimetres, so we decided to use $R = 10^{-2}m$ as a value representative of pipes flows.

We plotted on the same graph the evolution of Lamb vector divergence given by equation (35). The following figure gives four graphs obtained for (a) $K_{max} = 2000$; (b) $K_{max} = 4000$; (c) $K_{max} = 6000$; (d) $K_{max} = 10^6$.

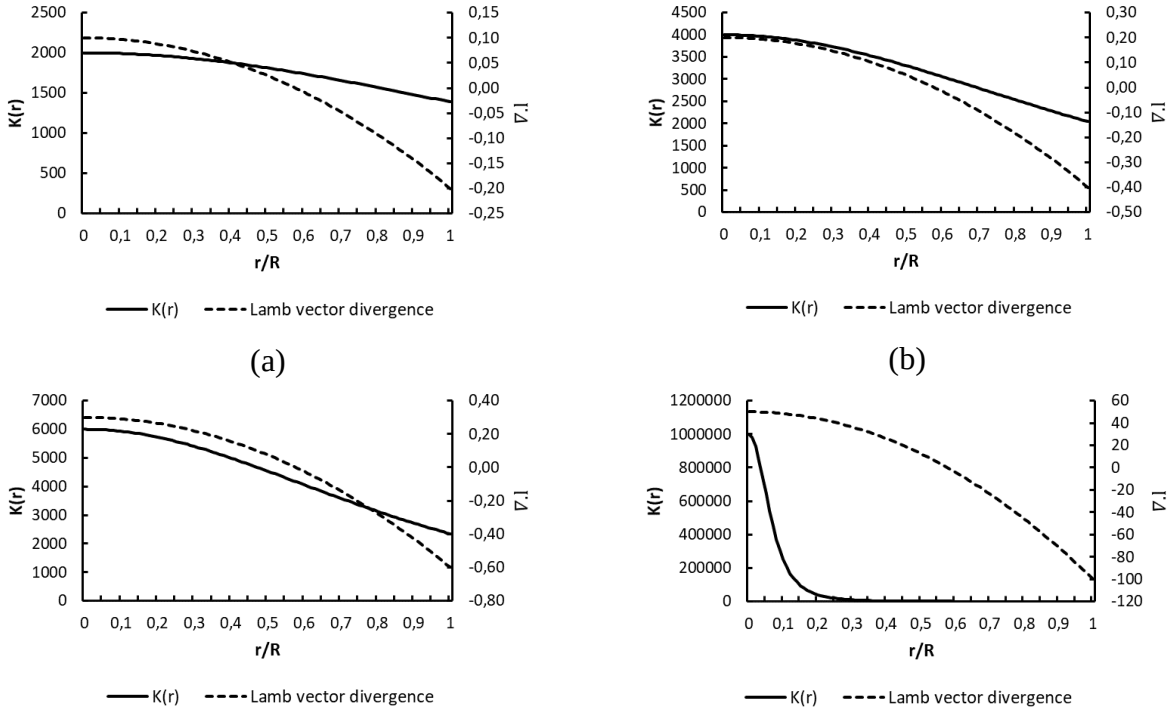

FIGURE 5: Evolution of $K(r)$ for several values of K_{max}: (a) $K_{max} = 2000$ – (b) $K_{max} = 4000$ –

(c) $K_{max} = 6000$ – (d) $K_{max} = 1\ 000\ 000$.

For $K_{max} = 2000$ (graph a) giving $K_{max}R^2 = 0.2$ in equation (35) and then $\boldsymbol{\nabla}.\boldsymbol{l} = -0.2$ at pipe wall, inflexion point exactly corresponds to the pipe wall explaining why it does not appear on the graph. The Lamb vector divergence $\boldsymbol{\nabla}.\boldsymbol{l}$ is represented by the dotted line and its values are given on the right-side axis. As discussed above, we have $\boldsymbol{\nabla}.\boldsymbol{l} = 0$ for $r = R/\sqrt{3}$ and this value does not change as K_{max} increases in graphs (b), (c) and (d).

In graph (a), it is clear that curvature of the POR does not change a lot as (r/R) increases from duct centre to the wall meaning that the POR is not sharp. It is quite easy to calculate a Reynolds number value from K_{max} using the following relationship:

$$Re = \frac{R^3}{2\nu}\sqrt{K_{max}} \qquad (39)$$

Of course, the use of this equation requires the knowledge of the fluid kinematic viscosity value. Considering the most common liquid encountered in experiments and industrial applications i.e. water at a temperature of 20°C, we have $\nu = 10^{-6}m^2.s^{-1}$ and we obtain $Re = \sqrt{K_{max}}/2$.
For $K_{max} = 2000$ it gives $Re \cong 22.4$ well corresponding to the laminar flow regime and then to a relatively flat POR with low Gauss curvature variation.

As the value of K_{max} increases in graphs (b), (c) and (d), and then the Reynolds number, the inflexion point moves from the right (wall) to the left (pipe centre). Graph (c) exactly corresponds to $r = R/\sqrt{3}$ where $\boldsymbol{\nabla}.\boldsymbol{l} = 0$, Reynolds number value calculated using above equations is $Re \cong 38.7$ which is also in the laminar flow regime. Graph (d) is obtained with $K_{max} = 10^6$ corresponding to $Re = 500$ and an inflexion point location near the pipe centre i.e. $r = R/10\sqrt{5} \cong 0.0447R$.

Using above relationships, we found that for water at 20°C flowing in a pipe of radius $R = 10^{-2}m$, the values of K_{max} giving Reynolds number between 2000 and 100 000 are respectively $16\ 10^6$ and $4\ 10^{10}$. These results correspond to the following range of values for the inflexion point location:

$$\frac{\sqrt{5}}{10^4} \leq \frac{r}{R} \leq \frac{\sqrt{5}}{200} \qquad (40)$$

These calculations clearly show that as Reynolds value increases, the curvature of the POR concentrates at the centre of the pipe due to the sharpening of the velocity field. In the same time, the Lamb vector divergence maximum and minimum value reaches $Max(\boldsymbol{\nabla}.\boldsymbol{l}) = K_{max}R^2/2 = 800\,;20000$ and $Min(\boldsymbol{\nabla}.\boldsymbol{l}) = -K_{max}R^2 = -1600\,;\ -40000$. Considering equation (30), these results also give the values of energy field curvature as the scalar Laplacian of the Bernoulli function. As it will be discussed below, this approach gives a new vision of phenomena when Reynolds number value reaches Re_c but it does not really explain what can trigger turbulence birth when $Re > 2000$. The evolution of $K(r)$ function as K_{max} increases or equivalently as Re increases (equation 39) clearly shows that values of Reynolds number such as $Re > Re_c$ are reached when the inflexion point is infinitely close to the pipe centre. From a geometrical point of view, it means that the POR is very sharp and then very close to a perfect cone with zero curvature at its sides which are straight lines and infinite curvature at its top which is a singularity. This situation well illustrated in above graph (d) where $K_{max} = 10^6$ giving $r/R = \sqrt{5}/50$ which is not very far from the limit value $\sqrt{5}/200$ given in the above inequality and which can be considered as the value where the POR is unstable enough to trigger turbulence birth. We will now analyse the major role of pipe radius suggested by equation (39)

4.2 Evolution of $K(r)$ with radius R.

As showed by equation (39), the Reynolds number defined using the maximum value of the POR curvature strongly depends on the pipe radius (power 3). In the following graphs, we fixed $K_{max} = 10^6$ and we increased the pipe radius: (a) $R = 10^{-3}$; (b) $R = 10^{-2}$; (c) $R = 10^{-1}$; (d) $R = 1\ m$.

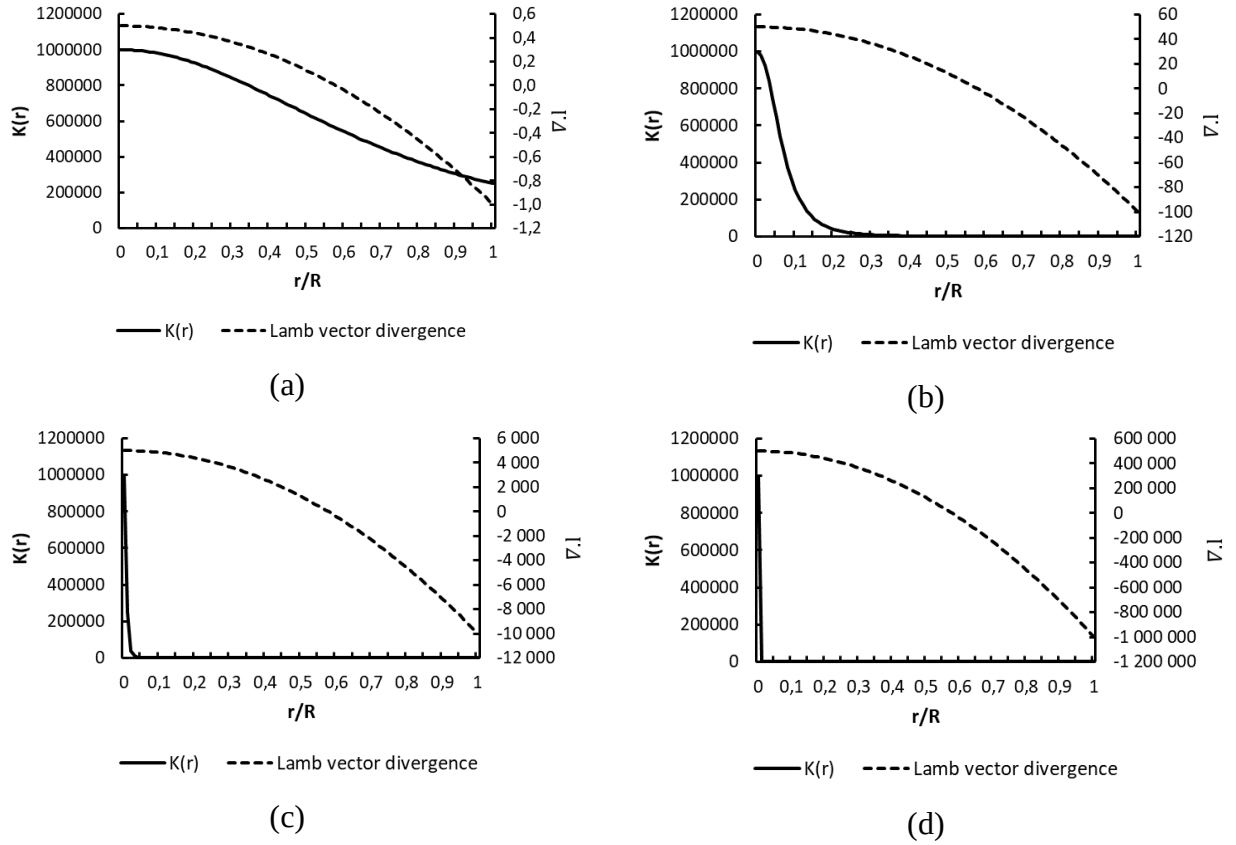

FIGURE 6: Evolution of $K(r)$ for several values of pipe radii.

Graph (b) corresponds to graph (d) in figure 5, i.e. $R = 10^{-2}$ and $K_{max} = 10^6$ ($Re = 500$). In graph (a), $R = 10^{-3}$ and inflexion point of $K(r)$ curve moved to the right, according to equation (39) which gives a large decrease of Reynolds number value ($Re = 50$) and then a much more stable flow. In graphs (c) and (d), the increase of pipe radius R gives a higher value of Reynolds number and then inflexion point moves to the left giving a turbulent flow. Reynolds number values (using the same kinematic viscosity than above i.e. $10^{-6} m^2 s^{-1}$) are respectively 510^5 and 510^8.

From these results, it is clear that, if we compare pipes flow stability at the same K_{max} value, i.e. for the same maximum curvature of the POR, the flow is much more stable in a capillary than in a pipe of large radius. This situation cannot be observed through classical approach i.e. using Reynolds number calculation giving the same critical value for a capillary or a pipe of 1 metre radius. The Reynolds number approach is very powerful for engineers who need to calculate the flow regime and then the pressure drops in a pipe whatever is its size. But this approach shows that, as a global flow parameter (involving only the mean velocity), it does not give details about the velocity field shape as the Gauss curvature function $K(r)$ does.

This result shows that $K(r)$ function and K_{max} could be used as a better parameter than critical Reynolds number to consider the fluid flow stability in pipes and also in ducts of arbitrary cross-section shape.

4.3 Discussion.

The first analysis of the results given in paragraph 4.1 is quite comparable to the classical analysis of Poiseuille flow stability in a pipe using critical Reynolds number values which depend on disturbances. The curvature approach only gives additional information about the mechanism that can trigger the turbulence i.e. a Gauss curvature concentrated at the centre of the pipe and a maximum value of Lamb vector divergence at this location.

Because most of experimental and numerical approaches consider fluids with a kinematic viscosity close to 10^{-6}m².s^{-1} and pipe radii in the range of 10^{-2}m, these results are in agreement with classical values found in sourcebooks.

But analysis performed in paragraph 4.2 clearly established the strong influence of pipe radius on the stability of Poiseuille flow. In a capillary, the flow appears to be much more stable due to the change of inflexion point location and also to the much lower value of maximum Lamb vector divergence. For a large radius pipe, both the Gauss curvature curve and the Lamb vector divergence reach large values which promote instability and then turbulence birth. From these considerations, it is clear that critical Reynolds number is not enough to well characterize and determine the flow stability and then the apparition of the transition flow regime.
By considering the flow of water, with kinematic viscosity $\nu = 10^{-6}\ m^2.s^{-1}$, in a pipe of radius $R = 10^{-2}\ m$, we showed that maximum Gauss curvature K_{max} can reach $4\ 10^{10}\ m^{-2}$ for Reynolds number value $Re = 10^5$. This curvature value gives a curvature radius of $5\ \mu m$, which exactly corresponds to well-known Kolmogorov scale reported in many source books [1]. This scale length was considered by Kolmogorov, as the size of the smallest aggregates in a turbulent flow giving rise to kinetic energy dissipation into heat.

It is also well-known that the value $Re = 10^5$ corresponds to a maximum value which can be reached by minimizing all disturbances in the flow (entrance effects, vibrations…). It is quite amazing that, this Reynolds number value, corresponds to a curvature radius value in the order of Kolmogorov scale. For Reynolds number values in the order of 2000, curvature radius is around $250\ \mu m$ which corresponds to aggregates giving maximum energy transportation.

From above considerations, it seems that when maximum Gauss curvature of the laminar Riemannian manifold reaches values giving curvature radii around $100\ \mu m$, the laminar flow, or more accurately the laminar velocity field, becomes unstable and then prone to turbulent "puffs" as measured by Durst & Unsal [9]. Moreover, when this value reaches Kolmogorov scale, i.e. around $5\ \mu m$, the flow starts to be turbulent (transition flow regime) even if the level of disturbances is extremely low or null. This limit could be considered as the scale where the parabolic flow field cannot be maintain further corresponding to Kolmogorov scale where dissipation into heat occurs.
These results reinforce the major role of Poiseuille flow velocity field topology measured by Gauss curvature in flow stability and then for turbulence birth in a viscous flow.

5. Conclusion.

In this paper, we considered the laminar velocity field in a pipe as a smooth Riemannian manifold. In a first chapter, we calculated both its mean and Gauss curvature as a function of fluid velocity and pipe radius. Maximum curvature arises at duct centre as expected from the shape of the laminar paraboloid of revolution. Then, we investigated the unsolved problem of laminar flow stability using the Lamb form of Navier-Stokes equation. Because the Lamb vector divergence is considered as a major quantity in complex flows [7], we established a relationship between this parameter and the Gauss curvature of the flow velocity field. From this equation, we showed that whatever is the flow curvature, the Lamb vector divergence always reaches zero at

radius $r = R/\sqrt{3}$. For radius values lower than this value, i.e. in the region of pipe centre, the Lamb vector divergence is positive. For values greater than $R/\sqrt{3}$, i.e. toward the pipe wall, the Lamb vector divergence is negative. From these considerations, the Lamb vector divergence appeared not able to explain why the laminar flow becomes unstable and then why it suddenly turns into the transition flow regime.

We decided then to explore the role of Gauss curvature function in turbulence birth. As established in the first chapter of this paper, this function depends on both the maximum Gauss curvature of the velocity field and the pipe radius. Using a fixed value of pipe radius, and increasing the maximum Gauss curvature, we showed that the shape of Gauss curvature function changes and can exhibit an inflexion point. When maximum Gauss curvature is low, curvature function is nearly flat all-over the pipe radius. As this quantity increases, inflexion point moves from the pipe wall to the pipe centre and curvature concentrates along pipe axis. From a geometrical point of view, it means that as the Reynolds number increases, the paraboloid of revolution converges toward a perfect cone giving a singularity at its top.

We also considered the case of a fixed value of maximum Gauss curvature and variations of the pipe radius. We showed that the decrease of pipe radius gives rise to a more stable laminar flow and that the increase gives rise to a less stable flow. From these results, it appeared that Reynolds number could not be appropriate to study and explain fluids flow stability even if it has a huge interest for engineering purpose. The Gauss curvature of the velocity field could be used as a useful tool to characterize the laminar flow stability. We clearly showed that a very high value makes the velocity unstable and then prone to turbulence birth.
Finally, a comparison between curvature radius values and Kolmogorov scales in the turbulent flow regime appeared interesting. It seems that the minimum value of this quantity obtained for Reynolds number value around 10^5 corresponds to Kolmogorov scale i.e. $5\ \mu m$. This result could explain why transition flow occurs around this Reynolds number without disturbances. The origin of turbulence birth could then be found in the topology of the velocity field reaching the limit curvature given by Kolmogorov scale. This conjecture could be checked using numerical simulation of both internal and external flows. Moreover, as an important consequence, pure one-dimension shear flow giving a null curvature should never give rise to turbulence.

References

[1] N. Midoux, 1993, Mécanique et Rhéologie des Fluides (Fluids Mechanics and Rheology). Tech & Doc Lavoisier. ISBN 2-85206-928-8.
[2] F. Delplace, 2018. Laminar flow of Newtonian liquids in ducts of rectangular cross-section an interesting model for both physics and mathematics. Int. J. of Theoretical and Mathematical Physics, vol. 8, n°2, p. 52-55.
[3] C. Villani, 2016. Synthetic theory of Ricci curvature bounds. Japanese J. of Mathematics, vol.11, issue 2, p. 219-263.
[4] F. Delplace, 2018. Fluids flow stability in ducts of arbitrary cross-section. J. of Modern and Applied Physics, vol.2, n°2, p. 10-15.
[5] H. -S. Dou, 2006. Mechanism of flow instability and transition to turbulence. Int. J. Non-Linear Mech., vol.41, n°4, p. 512-517.
[6] K.T. Trinh, 2010. On the critical Reynolds number for transition from laminar to turbulent flow. Arxiv/1007.0810.2010.
[7] Hamman C.W., Klewicki J.C. & Kirby R.M., 2008. On the Lamb vector divergence in Navier-Stokes flows. J. Fluid Mech., vol. 610, p. 261-284.
[8] S.W. Churchill, 1977. Friction factor equation spans all flow regimes. Chem. Eng. J., vol.7, p. 91-92.
[9] F. Durst & B. Unsal, 2006. Forced laminar to turbulent transition of pipe flows. J. Fluid Mech., vol. 560, p. 449-464.